

## Dinuclear Hg(II) complex of new benzimidazole-based Schiff base: one-pot synthesis, crystal structure, spectroscopy, and theoretical investigations

Youssra Doria Lahneche, Housseem Boulebd, Meriem Benslimane, Mustapha Bencharif & Ali Belfaitah

To cite this article: Youssra Doria Lahneche, Housseem Boulebd, Meriem Benslimane, Mustapha Bencharif & Ali Belfaitah (2019): Dinuclear Hg(II) complex of new benzimidazole-based Schiff base: one-pot synthesis, crystal structure, spectroscopy, and theoretical investigations, Journal of Coordination Chemistry, DOI: [10.1080/00958972.2019.1680833](https://doi.org/10.1080/00958972.2019.1680833)

To link to this article: <https://doi.org/10.1080/00958972.2019.1680833>

 View supplementary material 

 Published online: 25 Oct 2019.

 Submit your article to this journal 

 View related articles 

 View Crossmark data 



# Dinuclear Hg(II) complex of new benzimidazole-based Schiff base: one-pot synthesis, crystal structure, spectroscopy, and theoretical investigations

Youssra Doria Lahneche<sup>a,b</sup>, Housseem Boulebd<sup>a</sup>, Meriem Benslimane<sup>b</sup>,  
Mustapha Bencharif<sup>c</sup> and Ali Belfaitah<sup>a</sup> 

<sup>a</sup>Faculté des Sciences Exactes, Laboratoire Des Produits Naturels D'Origine Végétale et de Synthèse Organique, Université des Frères Mentouri-Constantine 1, Constantine, Algeria; <sup>b</sup>Unité de Recherche de Chimie de L'Environnement et Moléculaire Structurale, Université des Frères Mentouri-Constantine 1, Constantine, Algeria; <sup>c</sup>Faculté des Sciences Exactes, Laboratoire Des Matériaux, Université des Frères Mentouri-Constantine 1, Constantine, Algeria

## ABSTRACT

A new dinuclear complex,  $[\text{HgCl}_2\text{L}]_2$ , was prepared using a Schiff base derived from benzimidazole ( $\text{L} = [1-(1H\text{-benzo}[d]\text{imidazol-2-yl})\text{-N-(4-methoxyphenyl)ethan-1-imine}]$ ). The mercury complex was obtained in good yield by one-pot reaction under microwave irradiation from 2-acetylbenzimidazole and *p*-anisidine, followed by addition of  $\text{HgCl}_2$ . The Hg(II) complex has been characterized by single-crystal X-ray diffraction analysis, IR and UV-vis spectroscopy. The mercury complex is built up from a dinuclear unit related by an inversion center through two bridging chlorine atoms. Each mercury atom is coordinated by two N atoms of the Schiff base L, one terminal Cl atom and two bridging Cl atoms in a square pyramidal geometry. To support experimental data, theoretical calculations including molecular geometry, electronic transitions and vibration frequencies of the ligand and its complex in the ground state were carried out using the global hybrid (B3LYP) density functional. In addition, a qualitative description of excited states and charge transfer character of electronic transitions states were carried out by plotting the Natural Transition Orbitals (NTOs) for main states. Theoretical calculations are in good agreement with experimental values.

## ARTICLE HISTORY

Received 3 June 2019  
Accepted 23 September 2019

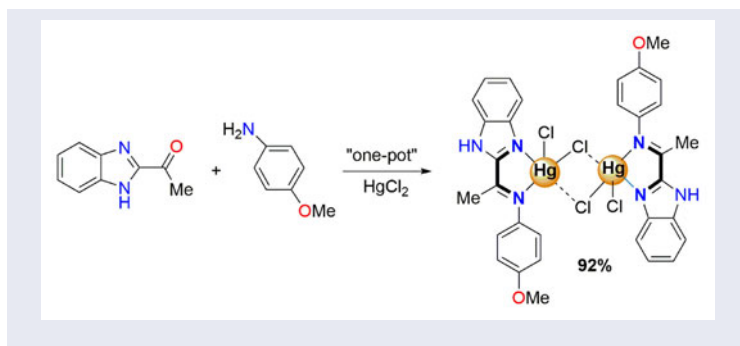
## KEYWORDS

Benzimidazole; Schiff base; Hg(II) complex; crystal structure; IR spectroscopy; UV-vis; spectroscopy; DFT calculations

**CONTACT** Mustapha Bencharif  [mustapha.bencharif@umc.edu.dz](mailto:mustapha.bencharif@umc.edu.dz); Ali Belfaitah  [abelbelfaitah@yahoo.fr](mailto:abelbelfaitah@yahoo.fr); [ali.belfaitah@umc.edu.dz](mailto:ali.belfaitah@umc.edu.dz)

 Supplemental data for this article is available online at <https://doi.org/10.1080/00958972.2019.1680833>.

© 2019 Informa UK Limited, trading as Taylor & Francis Group



## 1. Introduction

In recent years, the chemistry of azole-based ligand has known a considerable growth as proved by the increasing number of reports that highlight their properties as versatile N-donors in coordination chemistry [1–3], their structural novelty and their potential as new materials with biological importance [4]. The benzimidazole is an important nucleus containing two nitrogen atoms that can be found in some alkaloids such as Granulatimide [5]. Although rare in its natural state, this structural motif is also present inside our body as cobalt ligand in vitamin B12. In contrast, synthetic benzimidazole derivatives exhibited wide applications in various fields such as supramolecular ligands [6], medicinal drugs [7], biomimetic catalysts [8], agrochemicals [9], etc. In coordination chemistry, benzimidazole derivatives exhibited various coordination modes upon their ligation to metal ions [10, 11], and numerous corresponding complexes have been the subject of various biological applications such as antibacterial [12], anticancer [13], antioxidant [14], antifungal [15], anti-inflammatory [16], and enzyme inhibitor [17]. Benzimidazole complexes have also found some applications as catalysts [18].

Schiff bases derived from benzimidazole and their transition metal complexes were widely investigated as potential metallo-drugs because of their very easy synthesis with high yields and their strong ability to form stable coordination complexes with almost all metal ions [19]. These compounds exhibited remarkable biological activities [20, 21] and possess a flexibility to change and adapt their structure to a particular application in biological fields [22, 23].

The coordination chemistry of mercury was investigated by several research teams [24] due to the significant toxicological effects on living organisms and on the ecosystem we live in [25]. However, the mercury(II) compounds are used in various areas such as in paper industry, dyes, cosmetics, preservatives, fluorescent light bulbs, polymers, and to a lower extent, in mercury batteries [26]. Divalent mercury ion has a fully filled 5d orbital energy level (no unpaired electrons, 5d<sup>10</sup>), hence it possesses a strong tendency to form complexes easily. Metal complexes containing Hg(II) showed various structural arrangements, in which the metal ion exhibited various coordination numbers [26]. HgCl<sub>2</sub>L-type complexes, where L is a Schiff base containing two N donor atoms, invariably dimerize [27].

In line with our ongoing program devoted to the synthesis of new heterocyclic compounds containing imidazole derivatives or related compounds as main scaffold [28–31], we describe herein the synthesis and characterization of a new binuclear mercury complex containing a Schiff base derived from benzimidazole. This study includes an accurate and detailed description of structures, significant absorption bands assignments of IR and UV-vis spectra, molecular binding and other properties using the DFT method.

## 2. Experimental

### 2.1. Measurements and materials

IR spectra were recorded in the range of 4000–600  $\text{cm}^{-1}$  by means of a Jasco FT-IR 6300 type A spectrometer with ATR sampling accessory. UV-visible spectra were recorded in  $\text{CH}_3\text{CN}$  ( $10^{-5}$  M and  $10^{-3}$  M) on a UV-visible Jenway 6300 spectrophotometer. NMR spectra were recorded in  $\text{CDCl}_3$  on a Bruker Avance DPX250. Chemical shifts ( $\delta$ ) were given in ppm and J values in Hertz (Hz). The melting points were determined on a Kofler melting point apparatus and are uncorrected. All high-resolution mass spectra (HRMS) were recorded on a Bruker Maxis 4G at the CRMPO (Centre Régional de Mesures de Physiques l' Ouest, Rennes, France) using positive ion electrospray. Microwave irradiation experiments were performed with a microwave oven ( $P=300$  W). 2-Acetylbenzimidazole was prepared according to a literature procedure [32]. Commercial grade reagents were used as supplied: *o*-phenylenediamine (Alfa Aesar), lactic acid (Alfa Aesar), *p*-anisidine (Fluka),  $\text{HgCl}_2$  (Sigma-Aldrich). Acetonitrile was freshly distilled before use.

### 2.2. Synthesis

**2.2.1. Synthesis of *N*-(4-methoxyphenyl)-1-(1*H*-benzo[*d*]imidazol-2-yl)ethanimine (L)**  
0.5 mmol (80 mg) of 2-acetylbenzimidazole and 0.5 mmol (62 mg) of *p*-anisidine were placed into a sealed Pyrex-glass vessel and subjected to microwave irradiation with magnetic stirring for 4 min at 90 °C [33]. After cooling to room temperature, the resulting residue was purified by recrystallization from ethanol. Green crystals; 90%; M.p. 172–173 °C;  $^1\text{H}$  NMR (250 MHz,  $\text{CDCl}_3$ ),  $\delta$  (ppm): 10.68 (s, 1 H, NH), 7.89 (d,  $J=7.0$  Hz, 1 H, H7), 7.47 (d,  $J=7.0$  Hz, 1 H, H4), 7.41–7.31 (m, 2 H, H5, H6), 6.96 (dd,  $J=6.9, 2.2$  Hz, 2 H, H2', H6'), 6.89 (dd,  $J=6.9, 2.0$  Hz, 2 H, H3', H5'), 3.81 (s, 3 H,  $\text{CH}_3\text{-O}$ ), 2.46 (s, 3 H,  $\text{CH}_3$ );  $^{13}\text{C}$  NMR (62.9 MHz,  $\text{CDCl}_3$ ),  $\delta$  (ppm): 159.0, 157.0, 151.3, 143.9, 142.3, 133.7, 124.9, 122.8, 121.7, 120.8, 114.4, 111.4, 55.6, 16.5. ESI(+)-HRMS: Calcd. for  $[\text{C}_{16}\text{H}_{15}\text{N}_3\text{NaO}]^+ [\text{M} + \text{Na}]^+$ :  $m/z=288.11073$ . Found: 288.1110; FT-IR ( $\text{cm}^{-1}$ ): 3347, 3147, 3086, 2924, 2820, 1659, 1617, 1583, 1504, 1416, 1372, 1243, 1123, 1029, 960, 752; UV-vis ( $\text{CH}_3\text{CN}$ ),  $\lambda_{\text{max}}$  (nm): 236.5, 294, 339.5.

### 2.2.2. One-pot synthesis of di- $\mu$ -chlorido-bis-(chlorido-{(1*H*-benzo[*d*]imidazole-2-yl)ethanimino)-4-methoxy phenyl}mercury(II), $[\text{HgCl}_2\text{L}]_2$

Without isolation, the Schiff base prepared following the procedure above was dissolved in  $\text{CH}_3\text{CN}$  and treated with 0.5 mmol (137.7 mg) of  $\text{HgCl}_2$  salt in the same pot.

The mixture was stirred at room temperature for 5 min and the resulting precipitate was filtered off, washed with cold  $\text{CH}_3\text{CN}$  and dried in air to give the pure complex in 92% (245 mg) of yield. The structure determination of the dinuclear mercury complex  $[\text{HgCl}_2\text{L}]_2$  is based on an X-ray study of a suitable crystal obtained by slow evaporation at room temperature from a concentrated  $\text{EtOH}/\text{DMF}$  (2:1) solution. Yellow crystals, M.p.  $> 260^\circ\text{C}$ , FT-IR ( $\text{cm}^{-1}$ ): 3347, 3147, 3086, 2949, 2828, 1631, 1583, 1504, 1416, 1374, 1258, 1149, 1024, 960, 833, 752; UV-vis ( $\text{CH}_3\text{CN}$ ),  $\lambda_{\text{max}}$  (nm): 238.5, 296.5, 339.5.

### 2.3. Crystallographic analyses

A single-crystal of mercury complex was mounted under inert perfluoropolyether at the tip of a glass fiber and cooled under power nitrogen. The measurement was recorded on a Nonius Bruker APEXII diffractometer at 150 K with molybdenum  $\text{K}_\alpha$  radiation ( $\lambda = 0.71073 \text{ \AA}$ ).

The structure was solved using direct methods SIR92 [34] and refined by the least-squares method on structural factors  $F^2$  using SHELXL-2014 [35]. All hydrogens attached to carbons were placed in geometrically idealized positions, with C-H distances of 0.93  $\text{\AA}$  (aromatic), 0.96  $\text{\AA}$  (methyl) and refined using a riding model, with  $U_{\text{iso}}(\text{H}) = 1.5 U_{\text{eq}}(\text{C})$  for the methyl group and  $1.2 U_{\text{eq}}(\text{C})$  for the aromatic.

The design of the molecules was realized with the help of the software ORTEP-3 [36]. The crystal data and the refinement parameters of Hg(II) complex and pivotal geometric parameters related to coordination of metal ion together with intermolecular interactions hydrogen bonds, C-H... $\pi$  and  $\pi$ - $\pi$  stacking are summarized in Tables 1–3. Molecular structure of the complex is illustrated in Figure 1.

### 2.4. Computational methods

The theoretical study of the structure, electronic and optical properties was carried out in the framework of the density-functional theory (DFT) in gas phase, using the second-generation type of generalized gradient approximation (GGA), the global hybrid (B3LYP) [37]. The Hg atom was described through Stuttgart-Dresden effective core potential ECPs, designated as SDD. These energy-consistent ECPs are constructed to reproduce experimental observables of a single atom, such as ionization potentials and excitation energies, within the quasi-relativistic Wood and Boring theory [38]. The MWB60 pseudo-potential type implemented in Gaussian 09 was used for mercury atom. The 6-31+G(d) basis sets were used for nonmetal atoms (C, H, N, O) [39]. Further analyses of electronic and optical properties were performed by calculations of both vertical and adiabatic ionization potentials, the natural population analysis [40], and by the calculation of the UV-vis absorption in the framework of Time-Dependent DFT (TD-DFT) [41]. Excited states and charge transfer character of electronic transitions were characterized by plotting the electron density between the excited and ground states for the main peaks of natural transition orbitals (NTOs) [42]. All calculations have been performed using the Gaussian 09 version E.01 suite of programs [43].

**Table 1.** Crystallographic data and structure refinement parameters for [HgCl<sub>2</sub>L]<sub>2</sub>.

Empirical formula	C <sub>32</sub> H <sub>28</sub> Cl <sub>4</sub> Hg <sub>2</sub> N <sub>6</sub> O <sub>2</sub>
Formula weight	1071.58
Crystal size (mm)	0.15 × 0.1 × 0.05
Crystal morphology	Prism
Temperature (K)	293
Crystal system	Triclinic
Space group	<i>P</i> -1
<i>a</i> (Å)	8.5055(2)
<i>b</i> (Å)	9.8773(3)
<i>c</i> (Å)	11.2851(3)
$\alpha$ (°)	79.279(1)
$\beta$ (°)	68.938(1)
$\gamma$ (°)	71.366(1)
<i>V</i> (Å <sup>3</sup> )	835.64(4)
<i>Z</i>	1
D <sub>x</sub> (g cm <sup>-3</sup> )	2.129
Abs. coefficient (mm <sup>-1</sup> )	9.54
Transmission factors (min, max)	0.538, 0.746
$\theta$ Range (°)	2.7 to 27.5
Reflections measured	15768
Independent reflections; R <sub>int</sub>	3780; 0.018
Reflections with $I > 2\sigma(I)$	3486
Number of parameters	210
R( <i>F</i> ) [ $I > 2\sigma(I)$ ]	0.027
wR( <i>F</i> <sup>2</sup> ) (all data)	0.085
Goodness-of-fit on <i>F</i> <sup>2</sup>	1.18
$\Delta\rho_{\max,\min}$ (e Å <sup>-3</sup> )	1.30, -0.98

**Table 2.** Selected experimental and calculated bond lengths (Å) and angles (°) for [HgCl<sub>2</sub>L]<sub>2</sub>.

	Experimental	Calculated
Bond lengths (Å)		
Hg-N1	2.511(3)	2.725
Hg-N2	2.205(3)	2.380
Hg-Cl1	2.434(13)	2.431
Hg-Cl2	2.474(11)	2.606
Hg-Cl2 <sup>i</sup>	3.084(12)	2.897
Hg-Hg <sup>i</sup>	4.336(4)	4.054
Angles (°)		
N1-Hg1-Cl1	114.57(9)	97.08
N1-Hg1-Cl2	96.71(9)	86.31
N2-Hg1-Cl1	121.72(10)	122.04
N2-Hg1-Cl2	136.96(9)	136.78
Cl1-Hg1-Cl2	101.12(5)	99.01
N2-Hg1-N1	70.63(12)	66.96
N2-Hg1-Cl2 <sup>i</sup>	83.59(9)	96.38
N1-Hg1-Cl2 <sup>i</sup>	135.81(8)	159.84
Cl1-Hg1-Cl2 <sup>i</sup>	109.46(4)	101.60
Cl2-Hg1-Cl2 <sup>i</sup>	78.03(4)	85.24

Symmetry code: (i)  $-x + 2, -y + 1, -z$ .**Table 3.** Intermolecular interactions (Å, °) operating in the crystal structure for [HgCl<sub>2</sub>L]<sub>2</sub>.

	D-H	H...A	D...A	D-H...A	Symmetry
C5-H5—Cl2 <sup>ii</sup>	0.93	2.93	3.652(5)	135	$-x + 1, -y + 1, -z$
C17-H17B—Cl2 <sup>iii</sup>	0.96	2.92	3.798(6)	153	$-x + 2, -y, -z + 1$
C17-H17C—Cg1 <sup>iv</sup>	0.96	2.98	3.8932	159	$1 - x, 1 - y, 1 - z$
C17-H17C—Cg2 <sup>iv</sup>	0.96	2.78	3.6625	154	$1 - x, 1 - y, 1 - z$
Cg1—Cg1 <sup>v</sup>			3.5462		$1 - x, 1 - y, -z$

(Cg1: N2C2N3C4C9).

(Cg2: C4-C9).

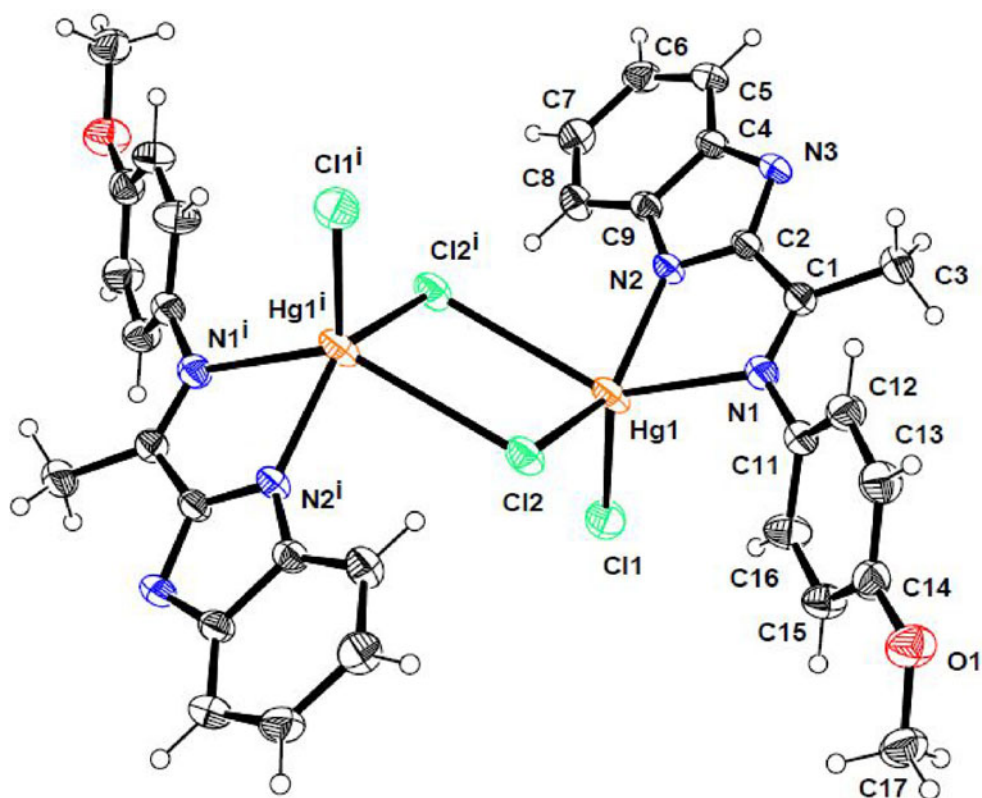


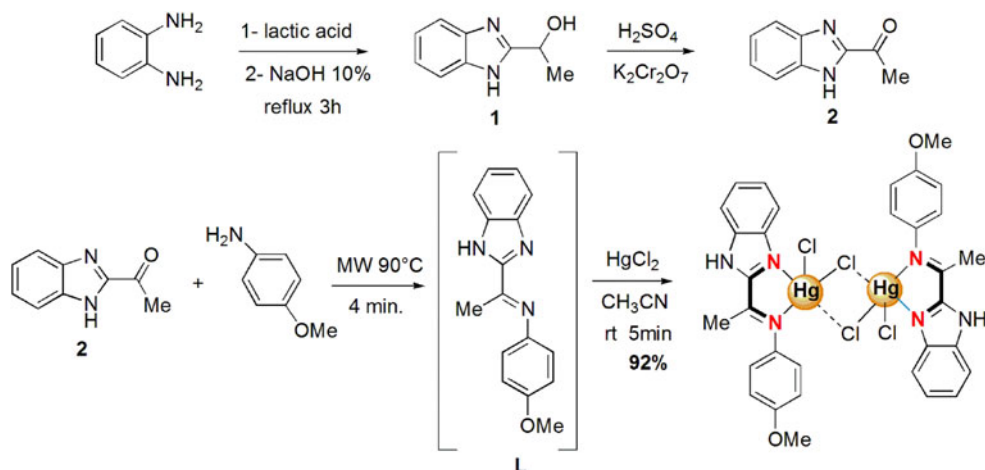
**Figure 1.** View of the molecular structure of  $[\text{HgCl}_2\text{L}]_2$ , with atom labeling. Displacement ellipsoids are drawn at the 40% probability level (hydrogens with arbitrary radii; blue: nitrogen, red: oxygen, green: chloride). Symmetry code: (i)  $2 - x, 1 - y, -z$ .

### 3. Results and discussion

#### 3.1. Synthesis

The 1-(1-*H*-benzo[*d*]imidazol-2-yl)ethan-1-one (2) was prepared in two steps according to the protocol described by Mathew *et al.* [32]. The addition of 1.5 equiv. of lactic acid to *o*-phenylenediamine furnishes the corresponding 1-(1-*H*-benzo[*d*]imidazol-2-yl) ethanol and subsequent oxidation reaction gives the 2-acetylbenzimidazole (Scheme 1).

The Hg(II) complex was prepared in two distinct steps: the synthesis of the Schiff base was followed by a complexation reaction. The benzimidazole-based-Schiff base was prepared by a reaction condensation of 2-acetylbenzimidazole with *p*-anisidine according to the procedure reported by Mermer *et al.* [33] (the NMR spectra of the Schiff base are illustrated Supplemental Figure S2). Subsequent addition of mercury chloride conducted in  $\text{CH}_3\text{CN}$  at room temperature gave the expected complex  $[\text{HgCl}_2\text{L}]_2$ . To optimize the yield, the sequence condensation/complexation was performed in a one-pot reaction (without isolation of the Schiff base) to give the mercury complex in excellent yield (92%). The dimeric compound is air stable with a high melting point. The molecular structure of the complex was characterized by IR and UV-vis spectroscopy, and by single crystal X-ray diffraction analysis. The synthetic pathway is outlined in Scheme 1.



Scheme 1. Synthesis of  $[\text{HgCl}_2\text{L}]_2$ .

### 3.2. Crystal structure description

The mercury complex crystallizes in the triclinic space group  $P\bar{1}$  (Table 1) with one half crystallographically independent molecule per asymmetric unit. The crystal structure is built up of a binuclear unit related around an inversion center through two bridging Cl atoms. The bridge is unsymmetrical with distances  $\text{Hg1-Cl2}$  2.474(11) Å and  $\text{Hg1-Cl2}^i$  3.084(12) Å, (i):  $2 - x, 1 - y, -z$ . The  $\text{Hg1} \dots \text{Hg1}$  separation is 4.336(4) Å (Table 2). We observe in the crystal structure that the Schiff base L acts as bidentate chelating agent through its two nitrogen atoms with the  $\text{Hg-N}_{\text{imino}}$  bond length (2.511(3) Å) longer than  $\text{Hg-N}_{\text{imidazol}}$  bond (2.205(3) Å) and the distance  $\text{Hg-Cl1}$  (2.434(13) Å) shorter than  $\text{Hg-Cl2}$  (2.474(11) Å). These results are in good agreement with those reported for similar compounds [27].

The  $\text{Hg}^{2+}$  ion is linked to the N atoms of the chelating ligand and to three Cl atoms resulting in the metal coordinated to five atoms. The coordination around the metal could be regarded as a quasi-regular square pyramidal geometry as quantified by the value of  $\tau_5 = 0.019$  with Cl2, Cl2<sup>i</sup>, N1, and N2 in the equatorial plane and Cl1 at the apical. The Hg1 atom is 0.929 Å out of the basal plane (Figure 1). The selected geometry parameters of  $[\text{HgCl}_2\text{L}]_2$  in the ground states were calculated in gas phase using B3LYP functional density and are in agreement with the experiments (Table 2). The calculated bond lengths are in good accordance with the experimental values within 0.002–0.214 Å. The calculated bond angles for the complex exhibit some differences compared to the experimental values with deviations within 0.18–24.03°. This result is can be explained by the fact that calculations have been carried out in gas phase. According to this observation, the calculations are in accordance with experiments. The optimized structure of  $[\text{HgCl}_2\text{L}]_2$  with atom numbering is shown in Supplemental Figure S1 in the Supporting Information, and optimized Cartesian coordinates are collected in Supplemental Table S1.

The crystal packing can be described as alternating layers parallel to the *ab* plane along the *b* axis, connected with weak intermolecular hydrogen bonding C-H... Cl (Figure 2; Table 3). The packing is also reinforced by two C-H...  $\pi$  interactions between the hydrogen

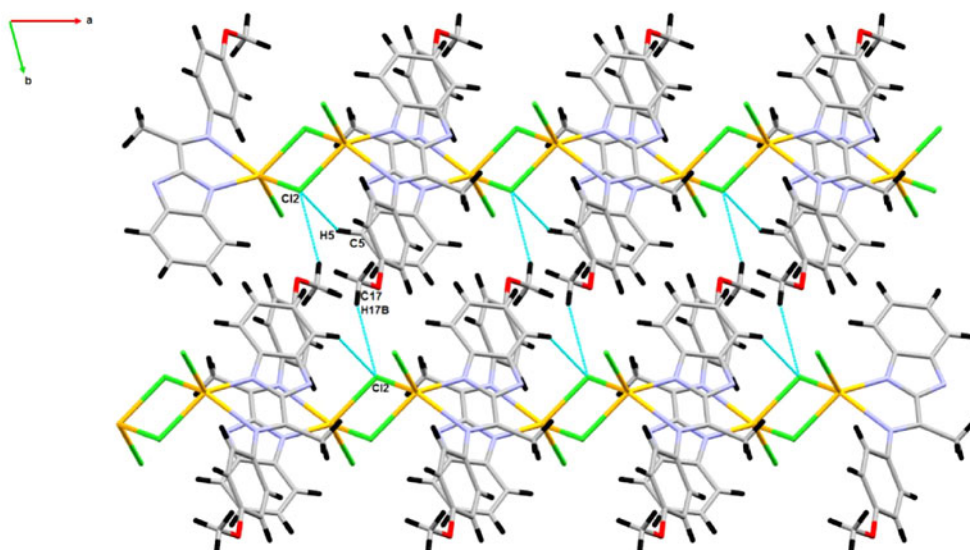


**Figure 2.** Hydrogen bonding network operating in the crystal packing of  $[\text{HgCl}_2\text{L}]_2$  viewed down the  $c$  axis.

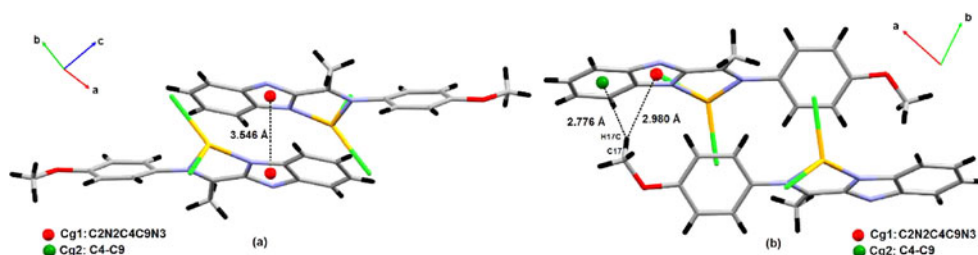


**Figure 3.** (a)  $\pi \dots \pi$  stacking and (b) C-H  $\dots \pi$  interactions operating in  $[\text{HgCl}_2\text{L}]_2$ .

atoms of methoxy group H17C and the  $\pi$ -system of the imidazole ring (H17C... Cg1 2.98 Å, C17-H17C... Cg1 159°) and with the  $\pi$ -system of the phenyl ring (H17C... Cg2 2.78 Å, C17-H17C... Cg2 154°) (Figure 3(b); Table 3). A  $\pi$ - $\pi$  stacking interaction Cg1... Cg1<sup>v</sup> (symmetry operation:  $(v) 1 - x, 1 - y, -z$ ) is also observed with centroid-centroid distance of 3.546 Å with a slippage of 0.429 Å and a dihedral angle of 0° (Figure 3(a); Table 3). These interactions link the layers together to build up a 3-D network.

### 3.3. Spectroscopic studies

#### 3.3.1. Infrared spectra

FTIR spectroscopy is an important tool for identifying the coordination nature of ligands with metal ions. To support experimental spectral data, significant absorption bands of IR spectra of L and  $[\text{HgCl}_2\text{L}]_2$  were calculated using the DFT/TD-DFT with B3LYP level as functional density. The spectrum of the free ligand L shows a broad weak band centered at  $3347\text{ cm}^{-1}$  attributable to  $\nu(\text{N-H})$  stretching vibration, very weak bands in the range  $3127\text{--}3086\text{ cm}^{-1}$  assignable to  $\nu(\text{C-H})$  aromatic, and two broad weak bands at  $2924$  and  $2820\text{ cm}^{-1}$  attributable to  $\nu(\text{CH}_3/\text{OCH}_3)$  asymmetric

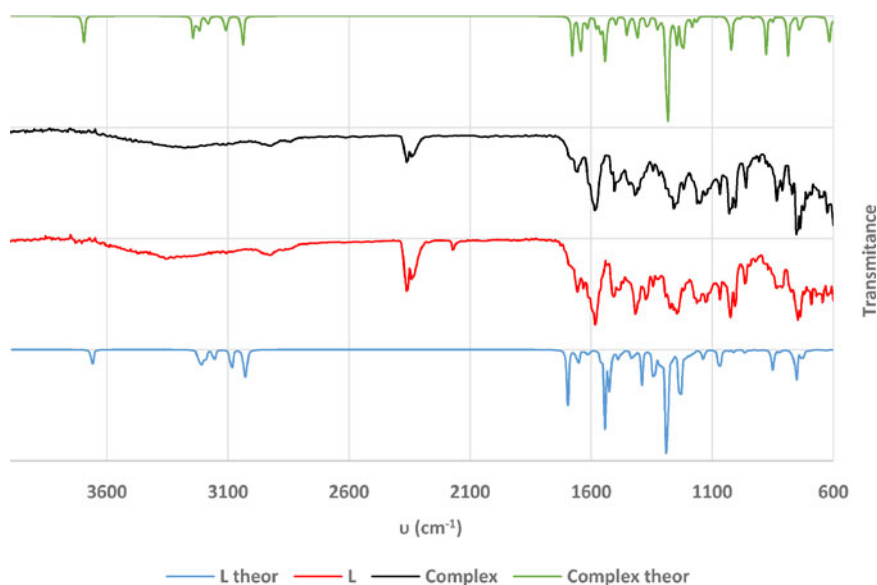


**Figure 4.** Overlapped experimental and theoretical IR spectra of the ligand (L) and  $[\text{HgCl}_2\text{L}]_2$ .

**Table 4.** Selected experimental and calculated vibrational frequencies ( $\text{cm}^{-1}$ ) using B3LYP functional for L and  $[\text{HgCl}_2\text{L}]_2$ .

Assignment	L		Complex	
	Exp.	Calculated	Exp.	Calculated
$\nu(\text{N-H})$ (stret.)	3347	3660	3347	3696
$\nu(\text{C-H})$ arom (stret.)	3147-3086	3223-3182	3147-3086	3244/3204
$\nu(\text{CH}_3)$ (stret.)	2924/2820	3157/3084	2949/2828	3038/3043
$\nu(\text{C=N})$ (stret.)	1659/1617	1697/1677	1631/[1604-1553]	1641-1561
$\nu(\text{C=C})$ (stret.)	1583	1543	1583	1618
$\nu(\text{CH}_3)$ (bend.)	1416/1372	1525-1491	1416/1374	1538/1453
$\nu(\text{C-O})$ (stret.)	1029	1070	1024	1023
$\nu(\text{C-H})$ arom (bend.)	960/752	848/754	960/752	877/788

stretching vibrations. Calculated frequencies occur at 3660, 3223–3182, and 3157/3084  $\text{cm}^{-1}$  for  $\nu(\text{N-H})$ ,  $\nu(\text{C-H})$  aromatic and  $\nu(\text{CH}_3/\text{OCH}_3)$  stretching vibrations, respectively [44]. Upon complexation to mercury ion, the peaks attributed to  $\nu(\text{N-H})$  and  $\nu(\text{C-H})$  aromatic remain practically intact, while  $\nu(\text{CH}_3/\text{OCH}_3)$  are slightly shifted at 2949/2828  $\text{cm}^{-1}$ , these bands are calculated at 3696, 3244–3204, and 3184/3167  $\text{cm}^{-1}$  for  $\nu(\text{N-H})$ ,  $\nu(\text{C-H})$  aromatic and  $\nu(\text{CH}_3/\text{OCH}_3)$  stretching vibrations, respectively. In the experimental spectra (Figure 4), the two broad medium bands of L at 1659 and 1617  $\text{cm}^{-1}$  attributable to the open-chain imino  $\nu(\text{C=N})$  and  $\nu(\text{C=N})$  stretching vibrations, respectively, underwent a bathochromic shift to 1631  $\text{cm}^{-1}$  and merged with  $\nu(\text{C=C})$  stretching vibrations in the range 1604–1553  $\text{cm}^{-1}$ , indicating the coordination of the imino- and imidazole-nitrogen atoms to the metal ion [45, 46]. The calculated frequencies with B3LYP occur at 1697 and 1677  $\text{cm}^{-1}$  for  $\nu(\text{C=N})$ , and 1641  $\text{cm}^{-1}$  for  $\nu(\text{C=N})$  for the complex (Figure 4). In the spectrum of the ligand, the strong broad band observed at 1583  $\text{cm}^{-1}$  was attributed to  $\nu(\text{C=C})$  stretching vibrations, and those observed at 1416/1372  $\text{cm}^{-1}$  were assigned to  $\nu_{\text{asym/sym}}(\text{CH}_3)$  bending vibrations. These bands remain practically intact for the complex and were calculated

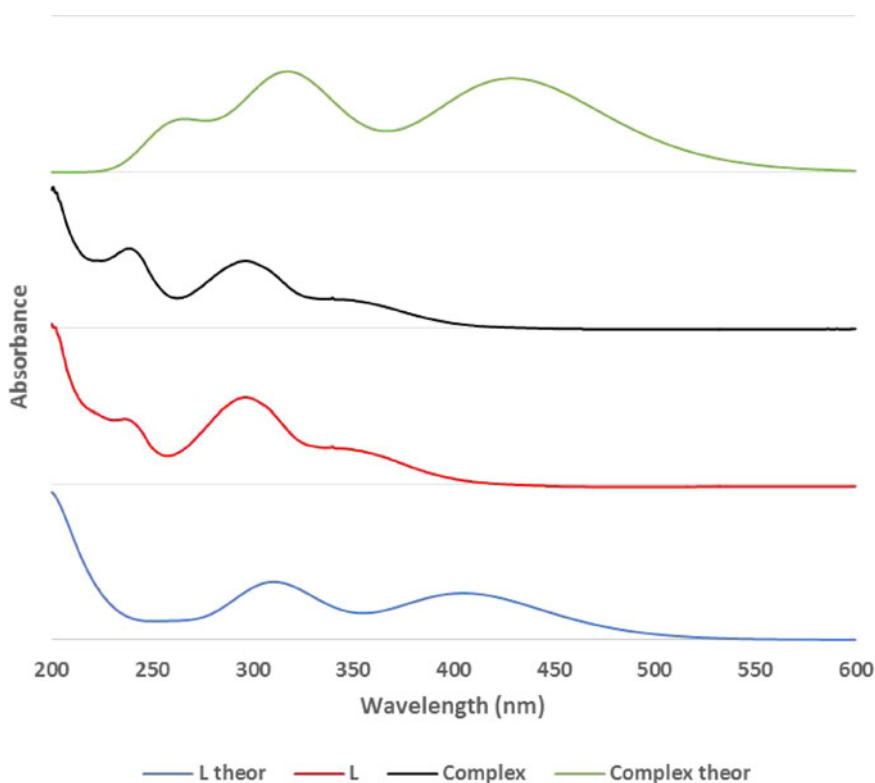


**Figure 5.** Overlapped experimental and theoretical UV-vis spectra of the ligand (L) and  $[\text{HgCl}_2\text{L}]_2$ .

at  $1543\text{ cm}^{-1}$  for  $\nu(\text{C}=\text{C})$  stretching vibrations, and  $1525/1491\text{ cm}^{-1}$  for  $\nu_{\text{asym/sym}}(\text{CH}_3)$  bending vibrations for L. The complex  $[\text{HgCl}_2\text{L}]_2$  calculations gave peaks at  $1618$  and  $1538/1453\text{ cm}^{-1}$  attributable to  $\nu(\text{C}=\text{C})$  and  $\nu(\text{CH}_3)$ , respectively. The sharp band observed at  $1029\text{ cm}^{-1}$  was slightly shifted at  $1024\text{ cm}^{-1}$  for the complex and was assigned to  $\nu(\text{C}-\text{O})$  stretching vibrations. It was calculated at  $1070\text{ cm}^{-1}$  for L and at  $1023\text{ cm}^{-1}$  for the complex. Finally, the sharp bands occurring at  $960$  and  $752\text{ cm}^{-1}$  are attributed to the in-plane and out-of-plane bending vibrations of C-H aromatic, respectively, for L, these bands remain unchanged for  $[\text{HgCl}_2\text{L}]_2$ . The calculated vibration frequencies are in good agreement with experimental data. The experimental and theoretical data are slightly different because calculations were carried out in gas phase. The IR spectral information thus supports the suggestion of the coordination of N atoms of L to the mercury ion. Overlapped experimental and theoretical IR spectra of the ligand (L) and the complex are pictured in [Figure 4](#), and major bands are summarized in [Table 4](#) together with the experimental values.

### 3.3.2. UV-vis study

Overlapped electronic experimental and theoretical spectra of the free ligand L and its corresponding complex  $[\text{HgCl}_2\text{L}]_2$  recorded at  $10^{-5}\text{ M}$  concentration in  $\text{CH}_3\text{CN}$  solution are shown in [Figure 5](#). The spectrum of L displays three broad absorption bands at  $\lambda_{\text{max}} = 236.5$  (I),  $296.5$  (II) and  $339.5\text{ nm}$  (III). Bands I, II, and III were attributed to

**Table 5.** Electronic transition orbitals of L and [HgCl<sub>2</sub>L]<sub>2</sub>.

	$\lambda_{\text{exp.}}$ (nm)	$\lambda_{\text{calcd.}}$ (nm)	E (eV)	Oscillator strength ( <i>f</i> )	Main transition states with major contribution (%)
L					
Band I	236.5	204.4	0.3528	0.3495	HOMO-1 → LUMO + 4 (49.51%)
Band II	296.5	312.2	3.9715	0.5103	HOMO-1 → LUMO (81.83%)
Band III	339.5	405.5	3.0578	0.5892	HOMO → LUMO (96.15%)
[HgCl <sub>2</sub> L] <sub>2</sub>					
Band I	238.5	262.45	4.7241	0.2070	HOMO-10 → LUMO + 2 (54.94%) HOMO-6 → LUMO + 2 (18.99%)
Band II	296.5	318.34	3.8948	0.9483	HOMO-4 → LUMO (36.28%) HOMO-5 → LUMO + 1 (37.64%)
Band III	339.5	429.36	2.8876	1.1889	HOMO → LUMO + 1 (49.49%) HOMO-1 → LUMO (46.74%)

intraligand  $\pi-\pi^*$  transitions [47]. Upon complexation, no change was perceived for absorption bands II and III of the Schiff base, while absorption band I was shifted to a slightly higher wavelength (236.5 nm → 238.5 nm). The calculated excited energies at the TD-DFT with B3LYP (Table 5) show that the ligand's well-resolved experimental absorption at 236.5 nm originating in the first excited transition state was attributed to HOMO-1 → LUMO + 4 with  $\pi-\pi^*$  character; this band was calculated at 204.4 nm. The broad absorption band observed at 296.5 nm (band II) was calculated at 312.2 nm, mainly involved HOMO-1 → LUMO transition state and was attributed to intraligand transition with  $\pi-\pi^*$  character. The weak absorption band centered at 339.5 nm (band III) was calculated at 405.5 nm and assigned to HOMO → LUMO transition state. For the complex two main transition states were involved for each absorption band with variable contributions (Table 5). Bands I, II, and III were calculated at 262.4, 318.3, and 429.3 nm, respectively. These bands correspond to: HOMO-10 → LUMO + 2/HOMO-6 → LUMO + 2 transitions attributed to a charge transfer from the ligand to the metal ion (LMCT) for band I, HOMO-4 → LUMO/HOMO-5 → LUMO + 1 transition states assigned to a metal-ligand charge transfer Hg(II) →  $\pi^*$  ligand (MLCT) for band II. Finally, band III mainly involved HOMO → LUMO + 1/HOMO-1 → LUMO transition states as intraligand charge transfer  $\pi-\pi^*$ . In 10<sup>-3</sup> M solution of the complex, none of metal-originated transition was observed. A schematic illustration of some selected molecular orbital transitions with the Kohn-Sham orbitals of [HgCl<sub>2</sub>L]<sub>2</sub> is expressed in Figure 6 and Supplemental Figure S3 and shows the contour plots of some selected molecular orbital transitions of L.

A qualitative description of electronic excitation states was carried out using the Natural transition orbitals (NTOs) [43]. The transitions associated with excited states were described by a substantial list of main transition states with major contributions. The NTOs analysis (Figure 6) showed a spin-allowed single-singlet electronic transition. An almost pure one natural orbital to one natural orbital transition was detected. As seen in Table 5, the natural orbital pairs contribute to the excitations with 49.51% at 236.5 nm, 80.83% at 296.5 nm and 96.15% at 339.5 nm for L. For the complex, the highest contribution is 54.94% at 262.4 nm, 37.54% at 318.3 nm and 49.49% at 429.3 nm. Experimental and calculated absorption wavelength  $\lambda$  (nm), excitation energy E (eV), oscillator strength (*f*), and main transition states with their major contribution (in percentage) of L and the complex are collected in Table 5.

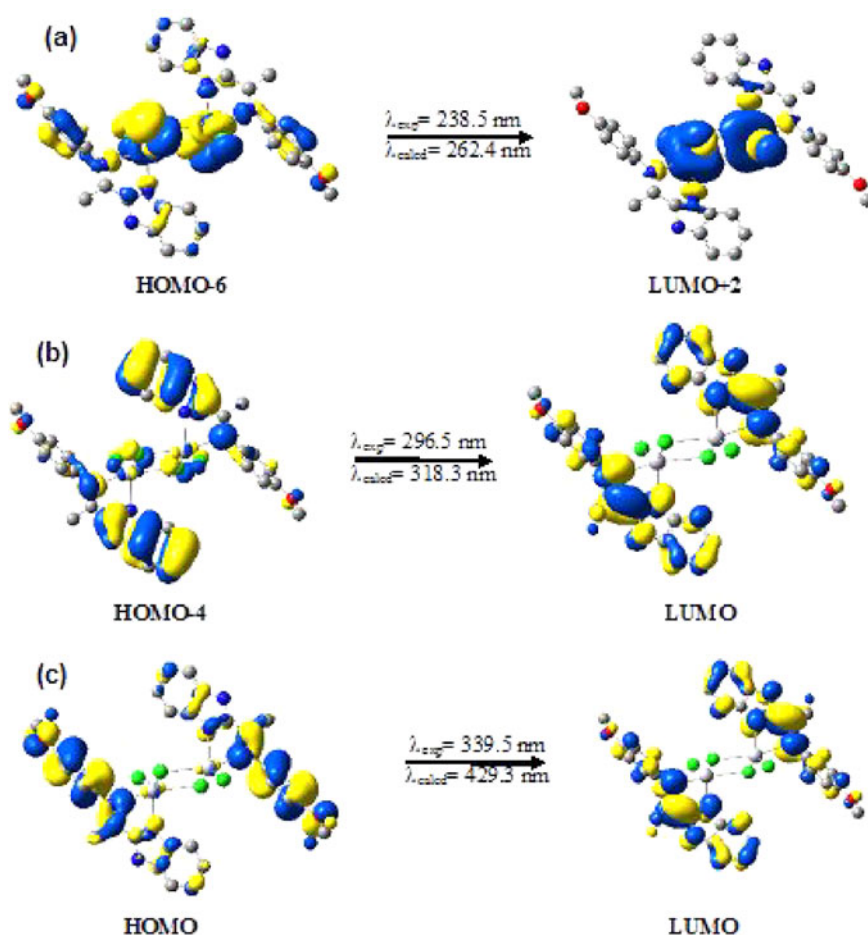


**Figure 6.** Schematic illustration of selected molecular orbital transitions of  $[\text{HgCl}_2\text{L}]_2$  with the Kohn-Sham orbitals corresponding to (a) LMCT, (b) MLCT and (c) intraligand charge-transfer  $\pi\text{-}\pi^*$ .

**Table 6.** NPA atomic charge distribution for  $[\text{HgCl}_2\text{L}]_2$  and L.

Atom	Complex	L
Hg	+0.467	–
N1 (imino)	–0.484	–0.009
N2	–0.587	–0.336
Cl1	–0.383	–
Cl2	–0.389	–

### 3.3.3. Frontier molecular orbitals

The HOMO and LUMO levels, called frontier molecular orbitals (FMOs), play an important role in the optical and electric properties, and in UV-vis spectra. The energy and electron density are an indicator of the stability, the chemical reactivity and the excitation properties of a molecule. The calculations were carried out in PCM solvent model. The HOMO and LUMO pictures with the contour plots and energy of selected frontier orbital energies of the complex and L are reproduced in [Supplemental Figure S4](#). As shown in [Supplemental Figure S4](#), the HOMO-LUMO energy gaps are 3.77 and 3.53 eV

for L and the complex, respectively. This intramolecular charge transfer belongs mainly to the local excitations  $\pi\text{-}\pi^*$ .

### 3.3.4. Other properties of the complex

Atomic charge distributions on atoms of the complex and L were calculated using B3LYP functional density and evaluated by natural population analysis (NPA) in gas phase. The calculated charge distribution on Hg(II) ion are lower than its formal charge of +2, while the electron density of N atoms as near-neighboring atoms slightly increased with respect to that of free ligand (Table 6). Electron transfer of N as donor atoms of the ligand (two nitrogen atoms) reduces the positive charge on the mercury atom from (+2) to (+0.464), indicating charge transfer between L and the Hg ion (Table 6). These results confirm that Hg(II) ion is coordinated to L across the nitrogen atoms.

To confirm some properties observed in the experiments such as stability and solubility, the total energy and dipole moment for the complex were calculated. The low value of the total energy of the mercury complex (−3863.964 Hartree) shows that it is stable with a high melting point, and the value of the dipole moment (0.0002 debye) indicates that it is not soluble in water and in polar solvent, as noted previously.

## 4. Conclusion

A new dinuclear Hg(II) complex derived from benzimidazole-based-Schiff-base has been synthesized and characterized by single-crystal X-ray analysis, IR and UV-vis spectroscopy.  $[\text{HgCl}_2\text{L}]_2$  is a dimeric complex in which each mercury atom is coordinated by two N atoms of the ligand, one terminal Cl atom and two bridging Cl atoms in a square pyramidal geometry. The geometry parameters, ground state structure, frontier molecular orbitals, IR as well as electronic spectral data of the ligand and the mercury complex were described by DFT and TD-DFT calculations using B3LYP functional levels, and are in good accordance with the experimental data.

## Acknowledgments

The authors thank Pr. A. Zertal at Laboratoire TIPE (Techniques Innovantes de Préservation de l'Environnement), Université des frères Mentouri-Constantine 1, Algeria, for the UV-vis recording, and Pr. B. Boudine at Laboratoire de cristallographie, department de physique, Université des frères Mentouri-Constantine 1, Algeria, for the IR recording. The authors are grateful to Dr. F. Berrée at Institut de Sciences Chimiques de Rennes (ISCR)-UMR CNRS 6226, *Chimie Organique et interfaces (COrint)*, Université de Rennes 1, France for elemental analysis.

## Disclosure statement

No potential conflict of interest was reported by the authors.

## Funding

This work was supported by MESRS (Ministère de l'Enseignement Supérieur et de la Recherche Scientifique), Algeria.

## ORCID

Ali Belfaitah  <http://orcid.org/0000-0003-0448-5810>

## References

- [1] A. Majumbar, U.P. Apfel, Y. Jiang, P. Moëne-Loccoz, S.J. Lippard. *Inorg. Chem.*, **53**, 167 (2014).
- [2] R. Rodriguez-Guttierrez, D. Macleod-Carey, X. Zarate, C. Bustos, E. Molins, E. Schott. *Polyhedron*, **81**, 414 (2015).
- [3] S.A. Deepthi, P. Ramesh, R. Trivedi, S.K. Buddana, R.S. Prakasham. *Inorg. Chim. Acta*, **435**, 200 (2015).
- [4] N. Ahmed, A.H. Chugtai, H.A. Younus, F. Verpoort. *Coord. Chem. Rev.*, **208**, 1 (2014).
- [5] R. Britton, J.H. de Oliveira, R.J. Andersen, R.G. Berlinck. *J. Nat. Prod.*, **64**, 254 (2001).
- [6] J.M. Hu, Y.G. Liu, Z.C. Hao, G.H. Cui. *J. Inorg. Organomet. Polym. Mater.*, **26**, 598 (2016).
- [7] M. Gaba, C. Mohan. *Med. Chem. Res.*, **25**, 173 (2016).
- [8] M. Devereux, D. O Shea, A. Kellett, M. McCann, M. Walsh, D. Egan, C. Deegan, K. Kędziora, G. Rosair, H. Müller-Bunz. *J. Inorg. Biochem.*, **101**, 881 (2007).
- [9] M. Tunçbilek, H. Göker, R. Ertan, R. Eryigit, E. Kendi, N. Altanlar. *Arch. Pharm. Pharm. Med. Chem.*, **330**, 372 (1997).
- [10] A. Benhassine, H. Boulebd, B. Anak, A. Bouraiou, S. Bouacida, M. Bencharif, A. Belfaitah. *J. Coord. Chem.*, **71**, 311 (2018).
- [11] F. Téllez, H. Lopez-Sandoval, S.E. Castillo-Blum, N. Barba-Behrens. *ARKIVOC*, **2008**, 245 (2008).
- [12] V.R. Mishra, C.W. Ghanavatkar, S.N. Mali, S.I. Qureshi, H.K. Chaudhari, N. Sekar. *Comput. Biol. Chem.*, **78**, 330 (2019).
- [13] T.S. Reddy, H. Kulhari, V.G. Reddy, V. Bansal, A. Kamal, R. Shukla. *Eur. J. Med. Chem.*, **101**, 790 (2015).
- [14] M. Özil, C. Parlak, N. Baltaş. *Bioorg. Chem.*, **76**, 468 (2018).
- [15] Y.B. Bai, A.L. Zhang, J.J. Tang, J.M. Gao. *J. Agric. Food Chem.*, **61**, 2789 (2013).
- [16] A.Ç. Karaburun, B. Kaya Çavuşoğlu, U. Acar Çevik, D. Osmaniye, B.N. Sağlık, S. Levent, Y. Özkay, Ö. Atlı, A.S. Kopardal, Z.A. Kaplancıklı. *Molecules*, **24**, 191 (2019).
- [17] S. Hirashima, T. Oka, K. Ikegashira, S. Noji, H. Yamanaka, Y. Hara, H. Goto, R. Mizojiri, Y. Niwa, T. Noguchi, I. Ando, S. Ikeda, H. Hashimoto. *Bioorg. Med. Chem. Lett.*, **17**, 3181 (2007).
- [18] A.I. Olivios Suarez, H. Jiang, X.-P. Zhang, B. de Bruin. *Dalton Trans.*, **4**, 5697 (2011).
- [19] G. Kumaravel, N. Raman. *Mater. Sci. Eng. C Mater. Biol. Appl.*, **70**, 184 (2017).
- [20] K. Mahmood, W. Hashmi, H. Ismail, B. Mirza, B. Twamley, Z. Akhter, I. Rozas, R.J. Baker. *Polyhedron*, **157**, 326 (2019).
- [21] A.A. Magd-El-Din, H.A. Mousa, A.A. Labib, A.S. Hassan, M.M. El-Ail, A.E. Ali, A.H. El-Rashedy, A. El-Desoky. *Z. Naturforsch.*, **C73**, 465 (2018).
- [22] N. Mishra, K. Poonia, S.K. Soni, D. Kumar. *Polyhedron*, **120**, 60 (2016).
- [23] L. Xia, Y.-F. Xia, L.-R. Huang, X. Xiao, H.-Y. Lou, T.-J. Liu, W.-D. Pan, H. Luo. *Eur. J. Med. Chem.*, **97**, 83 (2015).
- [24] (a) A. Kumar, M. Agarwal, A.K. Singh, R.J. Butcher. *Inorg. Chim. Acta*, **362**, 3208 (2009); (b) M. Montazerzohori, S. Jooari, S.A. Musavi. *Spectrochim. Acta, Part A*, **73**, 231 (2009); (c) S.M. Jahromi, M. Montazerzohori, A. Masoudiasl, E. Houshyar, S. Jooari, J.M. White. *Ultrason. Sonochem.*, **41**, 590 (2018).
- [25] (a) R.A. Bernhoft. *J. Environ. Public Health*, **2012**, 1 (2012); (b) M. McNutt. *Sciences*, **341**, 1430 (2013).
- [26] A. Morsali, M.Y. Masoomi. *Coord. Chem. Rev.*, **253**, 1882 (2009).
- [27] T.S.B. Baul, S. Kundu, H. Höpfl, E.R. Tiekinck, A. Linden. *Polyhedron*, **55**, 270 (2013).
- [28] H. Boulebd, L. Ismaili, H. Martin, A. Bonet, M. Chioua, J. Marco Contelles, A. Belfaitah. *Future Med. Chem.*, **9**, 723 (2017).

- [29] M. Bouchouit, M.E.H. Said, M. Kara-Ali, S. Bouacida, H. Merazig, N. Kacem-Chaouche, A. Chibani, B. Zouchoune, A. Belfaitah, A. Bouraiou. *Polyhedron*, **119**, 248 (2016).
- [30] H. Boulebd, S. Zama, B. Insaf, A. Bouraiou, S. Bouacida, H. Merazig, A. Romero, M. Chioua, J. Marco-Contelles, A. Belfaitah. *Monatsh. Chem.*, **147**, 2209 (2016).
- [31] A. Benhassine, H. Boulebd, B. Anak, A. Bouraiou, S. Bouacida, M. Bencharif, A. Belfaitah. *J. Mol. Struct.*, **1160**, 406 (2018).
- [32] B. Mathew, J. Suresh, S.J. Anbazhagan. *Saudi Chem. Soc.*, **20**, S132 (2016).
- [33] A. Mermer, N. Demirbas, H. Uslu, A. Demirbas, S. Ceylan, Y. Sirin. *J. Mol. Struct.*, **412**, 422 (2019).
- [34] A. Altomare, G. Cascarano, C. Giacovazzo, A. Guagliardi. *J. Appl. Crystallogr.*, **26**, 343 (1993).
- [35] G.M. Sheldrick. *Acta Crystallogr. C Struct. Chem.*, **C71**, 3 (2015).
- [36] L.J. Farrugia. *J. Appl. Crystallogr.*, **45**, 849 (2012).
- [37] (a) J. Trivado-Rives, W.L. Jorgensen. *J. Chem. Theory Comput.*, **4**, 237 (2008); (b) A.D. Becke. *Phys. Rev. A. Gen. Phys.*, **38**, 3098 (1988).
- [38] J.H. Wood, A.M. Boring. *Phys. Rev. B*, **B18**, 2701 (1978).
- [39] A.E. Reed, F. Weinhold. *J. Chem. Phys.*, **78**, 4066 (1983).
- [40] (a) A.E. Reed, R.B. Weinstock, F. Weinhold. *J. Chem. Phys.*, **83**, 735 (1985); (b) E. Runge, E.K.U. Gross. *Phys. Rev. Lett.*, **52**, 997 (1984).
- [41] (a) R. van Leeuwen. *Int. J. Mod. Phys. B*, **15**, 1969 (2001); (b) M.E. Casida. Time-dependent density-functional response theory for molecules. In *Recent Advances in Density Functional Methods. Part I*, D.P. Chong (Ed.), World Scientific, Singapore (1995).
- [42] R.L. Martin. *J. Chem. Phys.*, **118**, 4775 (2003).
- [43] Gaussian 09, Revision E.01, Gaussian, Inc., Wallingford, CT (2009).
- [44] J. Coates. In *Interpretation of Infrared Spectra, a Practical Approach. Encyclopedia of Analytical Chemistry*, R.A. Meyers (Ed.), Chap. 3, pp. 10820–10827, John Wiley & Sons Ltd. (2006).
- [45] P.E. Ikechukwu, P.A. Ajibade. *Molecules*, **20**, 9788 (2015).
- [46] T.S. Basu Baul, S. Kundu, S. Mitra, H. Höpfl, E.R.T. Tiekink, A. Linden. *Dalton Trans.*, **42**, 1905 (2013).
- [47] S. Demir, A. Güder, T.K. Yazıcılar, S. Çağlar, O. Büyükgüngör. *Spectrochim. Acta, Part A*, **150**, 821 (2015).